Thermal Strain Dependencies Characterizing Susceptibility of Steels to Cold Cracking

Thermal stress indices that determine cold-cracking probability in low- and medium-alloyed steel are investigated

BY B. S. KASATKIN AND S. B. KASATKIN

ABSTRACT. This article describes the procedure and results of investigation of the main thermal strain indices that determine the probability of cold cracking in welding of low- and medium-alloyed steels. The relationship has been established between the process of intensive relaxation of temporary stresses during structural transformations and initiation of microcracks in cooling under the conditions of welding thermal strain cycle. Parameter M_r has been suggested for estimation of steel susceptibility to cold crack formation. Effect of hydrogen on cold cracking is analyzed.

Introduction

Formation of cold cracks in welding of hardenable steels is caused by the effect of welding thermal strain cycle (WTSC) on welded joint metal that leads to complex changes in structure, saturation of weld metal and heat-affected zone (HAZ) with hydrogen redistribution of adverse impurities and alloying elements. The active mass transfer promotes weakening of metal and change in its structure due to the processes of grain boundary migration, recrystallization, high mobility of various segregating impurities and nonmetallic inclusions (Ref. 1). Cold cracks in welded joints are the result of mechanical fracture and therefore their formation is determined to a great degree by the peculiarities of the microplastic strain development under WTSC conditions. Microstructure of a welded joint, usually observed in sections cut out after welding, gives practically no information on the peculiarity of the kinetics of microplastic strain development. Such a problem can be solved only with simulation specimens tested under the conditions of the HAZ thermal strain (Ref. 2).

B. S. KASATKIN (deceased) and S. B. KASATKIN are with the E. O. Paton Electric Welding Institute of the Ukraine Academy of Sciences, Kiev, Ukraine.

Experimental Procedure

An experimental procedure was developed and a special installation MU-10 was manufactured that allowed study of the strain state and the microstructure under WTSC simulation conditions with various cooling rates using the restrained cylindrical specimens — Fig. 1. The installation was equipped with a chamber 7 that, if necessary, provides shielding of the polished specimen surface from air. The shielding atmosphere in the chamber is for vacuum and fills the chamber with pure argon. Such shielding enables observation of a complex pattern of microplastic strain and microfractures at the pre-polished specimen surface under WTSC conditions. Referring to Fig. 1, heating of the specimen (1) was performed by electric current from power source (9) through current leads (3). The heating temperature was 1250°C (2282 °F). Forces in the specimen were measured with a force measurement cell (4). During the test the changes in the temperature of the specimen-operating portion, the temporary stresses σ(t) (force P) and the acoustic emission were simultaneously recorded. All the results were sent to a computer to be registered and processed. Heating and cooling of the specimen were performed according to a preset program. Peculiarities of the thermal strain process and the microplastic strain fracture (microtears) were analyzed by examining the dynamics of the changes in the temporary stresses, the temperature, the acoustic emission and the microstructure. The cooling conditions were changed by purging the heated portion of the specimen with argon — Fig. 1. The stress concentration effect was estimated by using the results of testing the smooth and notched specimens — Fig. 2. Kinetics of changes in σ(t) in the restrained specimen during its cooling (Fig. 3) were determined by the following indices:

KEY WORDS

Medium-Alloyed Steel
Thermal Strain
Cold Cracks
Microplastic Deform
Deformation Fracture
Relaxation Rate
Acoustic Emission
Intergranular Slip
Intergranular Deformation
Hydrogen
Aluminum Alloys

- stress of intensive relaxation beginning and end σ_{rb} and σ_{re} (MPa);
- relaxation intensity factor $\Delta\sigma_r = \sigma_{rb} - \sigma_{re}$;
- residual stress σ_{res};
- relaxation rate $V_r = \Delta\sigma_r/t$, MPa/s;
- maximum relaxation rate $V_{r\,max}$, MPa/s;
- temperature (°C) of relaxation beginning and end, T_{rb} and T_{re};
- temperature (°C) of transformation beginning and end, T_{tb} and T_{te}.

The acoustic emission method provides useful information relative to the development of irreversible processes by using the personal computer to record AE signals.

The effects of the alloying system, the cooling conditions and the stress concentration were analyzed using the specimens of steels St. 3, 14C-2Cr-3/4Mn-1/2Mo-0.04B, 25C-2Cr-1Ni-1/2Mo-1/3V, 08C-18Cr-10Ni-1/2Ti, as well as 10C-1Cr-3/4Si-1/2Ni-1/2Cu and 20C-1Cr-1/2Mo.

Different stresses in specimens of

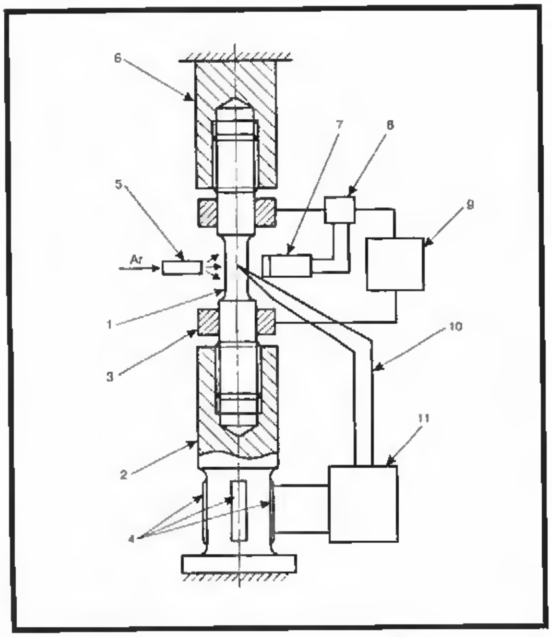

Fig. 1 — Diagram of installation MU-10. 2, 6 — restrained cooled clamps; 5 — purging for cooling; 8 — control unit for specimen heating source; 10 — thermocouple; 11 — oscillograph. (Remaining callouts noted in text.)

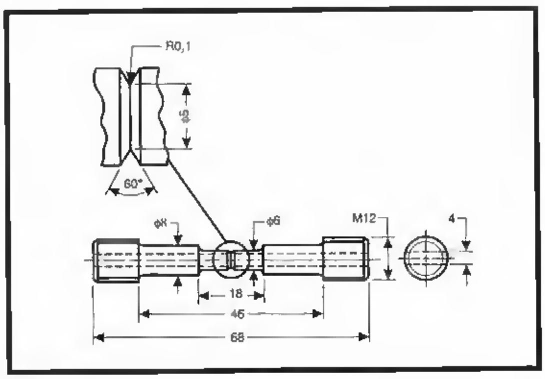

Fig. 2 — Test specimens with working portion 6 mm diameter, smooth or notched.

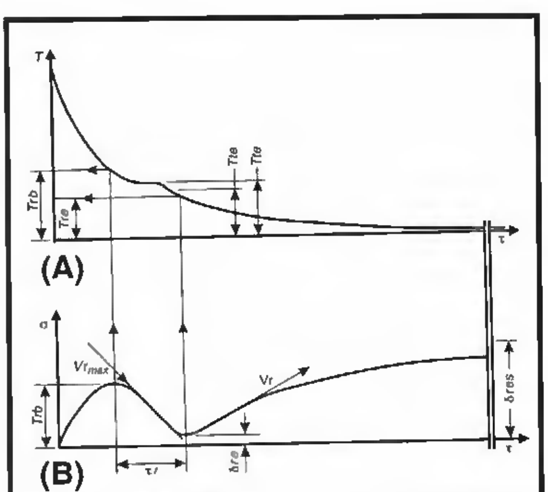

Fig. 3 — Temperature curve (A) and kinetics of stress development (B) for restrained specimen in cooling by WTSC.

these steels in simulation of a thermodeformational cycle of welding at a rigid fixation of the specimens are predetermined by the physical properties of the studied materials. The procedure does not provide an additional loading of specimens.

Results

Tests of the restrained smooth specimens (Fig. 4) revealed a marked difference in the kinetics of the changes in $\sigma(t)$ depending on the composition of steels under investigation: susceptible to cold cracking in welding (25C-2Cr-1Ni-1/2Mo-1/3V and 14C-2Cr-3/4Mn-1/2Mo-0.04B) and nonsusceptible, St. 3 and 08C-18Cr-10Ni-1/2Ti. The first group of steels is characterized by the relatively high level of σ_{rb} (more than 100 MPa), T_{rb} (less than 500°C [932°F]) and σ_{res} lower than the yield point σ_y for these steels. The St. 3 specimens have the low level of σ_{rb}, at T_{rb} = 700°C and $\sigma_{res} = \sigma_t$, for steel 08C-18Cr-10Ni-1/2Ti the continuous growth of $\sigma(t)$ up to the level of σ_{res} is observed in cooling.

Going from the smooth specimens to the notched ones and changing the cooling rate (within the ranges of 800–500°C [1472–932°F], without argon purging 40°C/s [104°F/s], and with argon purging 70°C/s [158°F/s] for steels 25C-2Cr-1Ni-1/2Mo-1/3V and 14C-2Cr-3/4Mn-1/2Mo-0.04B) led to an increase in σ_{rb}; however, the reaction of St. 3 to these changes was insignificant — Fig. 5. Apparently, the cause of cold crack initiation cannot be related to the level of σ_{res}; more likely, this cause exists in the development of intensive plastic strain during relaxation, in the increase in σ_{rb} and the shift of T_{rb} to the area of the lower temperatures. Figure 6 shows dependencies of $V_{r\ max}$ and σ_{rb} on the average temperature, T_{av}, of the $\gamma \rightarrow \alpha$ transformation interval and T_{rb} for the steels studied at different variants of testing the specimens. As seen from Fig. 6A, the increase in cooling rate of the smooth specimens (argon purging) led to the growth of $V_{r\ max}$ from 20 to 25 MPa/s (25C-2Cr-1Ni-1/2Mo-1/3V) and from 27 to 36 MPa/s (14C-2Cr-3/4Mn-1/2Mo-0.04B). Here, these changes for steel St. 3 are much weaker. Cooling rate exerts a marked effect on the shift of T_{tb} for the steels studied (by 80–100°C [176–212°F]). The presence of a notch in a specimen causes an increase in $V_{r\ max}$ and σ_{rb} — Fig. 6. The particularly great increase in $V_{r\ max}$ (up to 50 MPa/s) is observed in accelerated cooling (purging) of the notched specimens of steels 25C-2Cr-1Ni-1/2Mo-1/3V and 14C-2Cr-3/4Mn-1/2Mo-0.04B — Fig. 6A.

The high rates of stress relaxation and, therefore, of the plastic strain development at the simultaneous shift of the weakening process to the region of the lower temperatures (steel 25C-2Cr-1Ni-1/2Mo-1/3V, notched specimens, purging) are indicative of the intensive development of microplastic strains along the grain boundaries. Development of the microplastic strains causes difficulty in the accommodation of grains in joint plastic strain and leads to disturbance of the boundaries, structures, *i.e.*, to the formation of delayed fracture centers (Ref. 3).

On the other hand, the low rates of stress relaxation $V_{r\ max}$ and high temperatures of $\gamma \rightarrow \alpha$ transformation for steel St. 3 drastically change the general picture of the strain development; here, the microplastic strain develops both along the grain boundaries and inside the grains, greatly favoring the process of grain accommodation at the general plastic strain. Comparing the positions of the regions (on the coordinates of σ_{rb} – T_{rb}) for steel St. 3 and steels 14C-2Cr-3/4Mn-1/2Mo-0.04B and 25C-2Cr-1Ni-1/2Mo-1/3V (Fig. 6B) shows that the risk of cold cracking is caused not only by T_{rb} but also by the level of σ_{rb}.

The effects of the alloying system for the steels studied and of the specimen test conditions on the relationship between $V_{r\ max}$ and $\Delta\sigma_r$ are shown in Fig. 7. A significant difference in position of zones $\Delta\sigma_r$ – $V_{r\ max}$ for St. 3 and steels 14C-2Cr-3/4Mn-1/2Mo-0.94B, 25C-2Cr-1Ni-1/2Mo-1/3V is observed. The increase in cooling rate (purging of specimens), as well as the presence of stress concentrator (notch), have insignificant influence on the properties of St. 3; therefore, the scatter of points is small. Under similar conditions of specimen tests, zone $\Delta\sigma_r$ – $V_{r\ max}$ of steels 14C-2Cr-3/4Mn-1/2Mo-0.04B and 25C-2Cr-1Ni-1/2Mo-1/3V has large sizes. Hence, the influence of the notch is noticeably observed. A zone $\Delta\sigma_r$ – $V_{r\ max}$ for

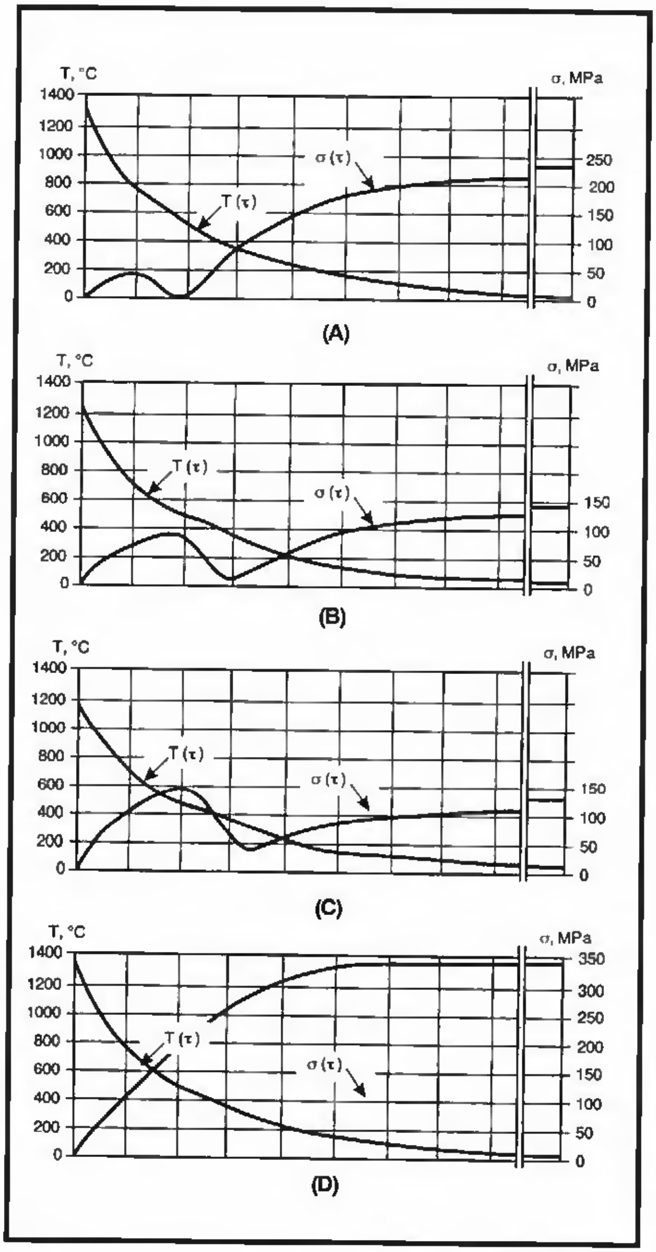

Fig. 4 — Effect of alloying system on kinetics of σ(t) development in restrained specimens in simulated WTSC. A — Steel St. 3; B — 14C-2Cr-3/4Mn-1/2Mo-0.04B; C — 25C-2Cr-1Ni-1/2Mo-1/3V; D — 08C-18Cr-10Ni-1/2Ti.

steels 14C-2Cr-3/4Mn-1/2Mo-0.04B and 25C-2Cr-1Ni-1/2Mo-1/3V can definitely be divided into two parts, confirming the existing concepts about the influence of stress concentrator (notch defect) on the process of cold cracking.

By analyzing the received data one concludes that, under the conditions of continuous cooling in WTSC, the values of $\Delta\sigma_r$ characterize the store of elastic energy, which is realized with the rate of V_r during relaxation process. The lower the T_{rb}, the larger the store of accumulated energy and the rate of its realization. Hence, the probability of cold cracking in welding is increased. On the basis of received dependencies, the parameter characterizing the relaxation intensity under WTSC conditions is suggested as

$$M_r = \Delta\sigma_r \cdot V_{r\,max}/T_{rb}.$$

Table 1 gives the parameters M_r for several grades of steels differing in susceptibility to cold-crack formation in welding. This table also gives the characteristic P_{cm} and basic data, characterizing the intensity of relaxation within the temperature range of $\gamma \rightarrow \alpha$ transformations. Notched specimens were tested — Fig. 2. Test conditions of the specimens are as follows: heat to 1200°C (2192°F), soak time 10 s, air cool at a rate of 40–45°C/s (104–113°F/s) within the interval from 800–500°C (1472–932°F).

A significant increase of M_r is observed when going from the group of steels without limits in the welding (St. 3, 09C-2Mn-3/4Si and 10C-1Cr-3/4Si-1/2Ni-1/2Cu) to the steels, in which cold cracking is probable (20C-1Cr-1/2Mo and others). The increase in M_r indicates it is necessary to make some additional technological arrangements, *i.e.*, preheating, elimination of long metal overheating, limitation of content of H, S, P, etc., to avoid cold-crack formation.

An essential confirmation is that the development of intensive relaxation and, hence, the M_r parameter are related to the drastic activation of microplastic strain and probability of sub-microcrack initiation in acoustic emission of the specimens deformed under WTSC conditions. The energy transferred by the AE waves is known to be correlated with the energy of various stages of microplastic strain and fracture (Ref. 4). The intensity of AE grows with the increase in the strain and crack rates. The spectrum of the AE waves depends greatly on the realized store of elastic energy. In the tests conducted, the store of elastic energy is determined by the value $\Delta\sigma_r$ and the intensity of its realization by V_r.

Two parameters were used for the analysis of the AE results, *i.e.*, number and amplitude of pulses. However, due to the limited potentialities of the equipment, the high amplitudes of the AE pulses were registered with some limitation; therefore, AE was mostly estimated by the number of pulses. Limit-at-signal input by the amplitude is up to 58 mV.

Measurement of AE with the specimens of the steels given in Table 2 show that the maximum peak of the sum of the events (pulses) coincides with the development of intensive relaxation on the temperature curve of cooling.

Two peaks of the sum of events are observed for the steels susceptible to quenching (T_{rb} < 500°C [932°F]); *i.e.*, the first one, having the lower value, is followed by the second, having the higher values of sum of AE events in the period of intensive relaxation — Fig. 8. The presence of the two peaks is associated with the wide range of structural $\gamma \rightarrow \alpha$ transformations and microplastic strain. The end of the intensive relaxation process (σ_{re}) is accompanied by the drastic drop of the acoustic pulses. Statistical analysis

Table 1 — Data on the Rate of Relaxation Within the Temperature Range of $\gamma \leftarrow \alpha$ Transformations for Notched Samples of Different Steels

N	Grade of steel	P_{cm}	Intensive Relaxation			
			$\Delta\sigma_r$, MPa	T_{rb}, °C	$V_{r\,max}$, MPa/s	M_r
1	St. 3	0.26	42	703	11.1	0.66
2	09C-2Mn-3/4Si	0.26	63	660	16.3	1.5
3	10C-1Cr-3/4Si	0.29	54	674	15	1.2
4	20C-1Cr- 1/2Mo	0.37	108	527	22.1	4.5
5	25C-2Cr-1Ni-1/2Mo-1/3V(a)	0.42	118	430	18.8	4.8
6	25C-2Cr-1Ni1/2Mo-1/3V	0.43	138	403	20	6.8

(a) Silicon-free steel, vacuum carbon deoxidized.

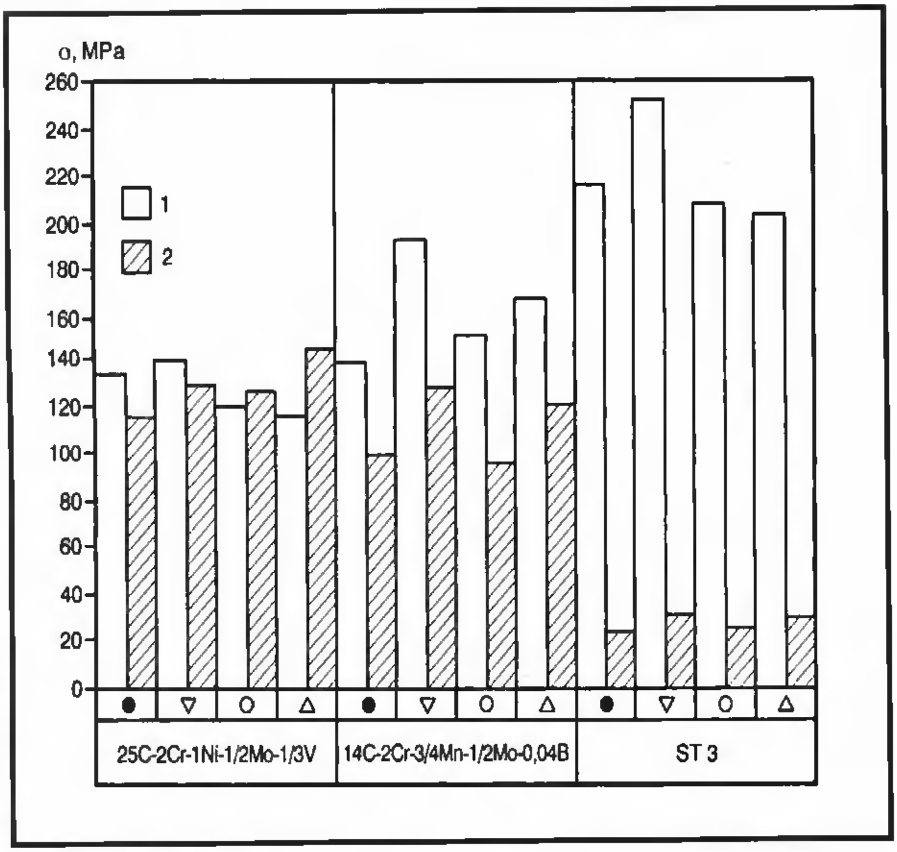

Fig. 5 — Effect of steel alloying system and specimen cooling conditions on σ_{res} (1) and σ_{rb} (2). • — smooth specimens, cooled without purging; o — same with purging; ∇ — notched specimens cooled without purging; Δ — same with purging.

of received acoustograms — with definition of the sum of events before and at the moment of intensive relaxation — was carried out. Four parameters were defined:

- $N_{b\ max}$ — Maximum number of events per second (pulse/s);
- N_b — Total number of events before the beginning of intensive relaxation (pulse);
- $N_{r\ max}$ — Maximum number of events per second (pulse/s);
- N_r — Total number of events in intensive relaxation.

The results of AE analysis for several steels are given in Table 2. In steels St. 3, 09C-2Mn-3/4Si, 10C-1Cr-3/4Si-1/2Ni-1/2Cu with relatively small values of M_r and high values of T_{rb}, peak values of N_r and $N_{r\,max}$ are observed at the moment of relaxation, related with $\gamma \rightarrow \alpha$ transformations. In steels with high values of M_r and $T_{rb} < 550°C$ (1022°F) — 20C-1Cr-1/2Mo, 25C-2Cr-1-Ni-1/2Mo-1/3V — AE is activated in the pre-relaxation period. It indicates the beginning of restructuring (bainite, acicular ferrite, etc.) and activation of microplastic strain. After achieving the peak values, the discrete microprocess is drastically reduced and then started again, heated to T_{rb} temperature and σ_{rb} stress level. Hence, the largest intensification of AE is achieved with $V_{r\ max}$. Then, a quick drop of emission at σ_{rb} occurs. The second maximum of AE (N_r and $N_{r\ max}$), caused by intensive relaxation, is, as a rule, higher than the first one, especially on steels 25C-2Cr-1Ni-1/2Mo-1/3V silicon-free steel and 25C-2Cr-1Ni-1/2Mo-1/3V, susceptible to hardening. It indicates that, with reduction of T_{rb} temperature and increase of M_r, the basic volume of microplastic strain and structural transformations occur during the period of intensive relaxation.

The results of AE analysis were supplemented with the investigation of the structure and peculiarities of microplastic strain under WTSC conditions. For this purpose, the specimens of 25C-2Cr-1Ni-1/2Mo-1/3V steel with polished working surface were tested. The 4-mm thick plane specimens were produced by additional treatment of round specimens with a sharp notch (Fig. 2) from two diametrically opposite sides (along dotted line). A special chamber protected the specimen surface from the air effect. Before heating the specimen, a vacuum of up to 1.33 Pa was created; after that the chamber was filled up with high-purity passing argon up to 120 kPa. The conditions of specimen heating-cooling are as follows: 1250°C (2282°F), soak time is 8 s, purging of specimen with argon jet, directed to the working part of the specimen.

Figure 9 shows the dynamics of changing the temporary stresses and temperature during the heating-cooling period of restrained specimen. The rate of specimen cooling was relatively high, 60°C/s (140°F/s) within the limits of 800–500°C (1472–932°F), T_{tb} = 330°C (626°F), T_{te} = 290°C (554°F). From the beginning of cooling, the tensile stresses were gradually increased. At a temperature of 440°C (824°F) they reach 79 MPa (tensile force is 1.5 kN), then a drastic drop occurred and, at a temperature of 275°C (527°F), the stresses reached values close to zero. The average rate of

Table 2 — Data on the Measurement of Acoustic Emission During Relaxation in Notched Samples of Different Steels

			Before Relaxation				In the Interval of Relaxation	
Grade of Steel	P_{cm}	M_r	σ(t), MPa	T, °C	$N_{b\ max}$ Pulse/s	N_b Pulse	$N_{r\ max}$ Pulse/s	N_r Pulse
St. 3	0.26	0.66	—	—	—	—	245	1006
09C-2Mn-3/4Si	0.27	1.5	—	—	—	—	315	1884
10C-1Cr-3/4Si-1/2Ni-1/2Cu	0.29	1.2	—	—	—	—	174	912
20C-1Cr-1/2Mo	0.37	4.5	72	692	208	1461	206	1735
25C-2Cr-1Ni-1/2Mo-1/3V	0.42	4.8	78	614	167	1430	387	3070
25C-2Cr-1Ni1/2Mo-1/3V	0.43	6.8	104	600	159	1109	371	2870

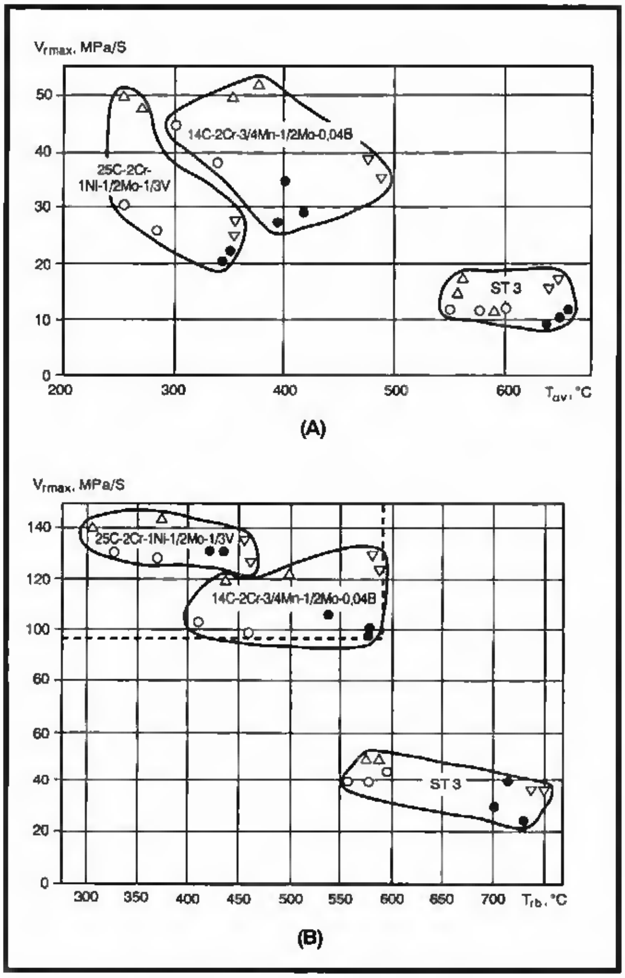

Fig. 6 — Effect of steel alloying system and temperature on: A — $V_{r\,max}$; B — σ_{rb}. (Designations, see Fig. 5.)

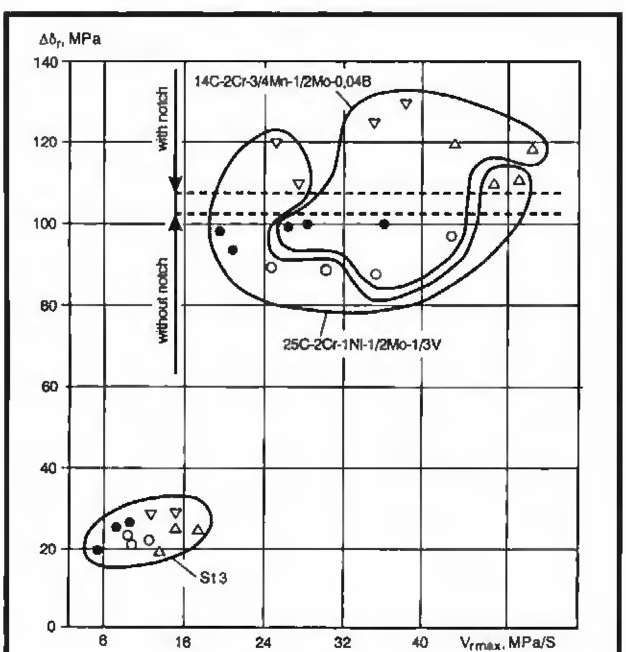

Fig. 7 — Effect of steel alloying system on the dependence of $\Delta\sigma_r$ relaxation characteristic on the rate of relaxation $V_{r\,max}$. (Designations, see Fig. 5.)

stress relaxation is 13.4 MPa/s; maximum rate is 21 MPa/s. Note that the temperature range of stress relaxation is sufficiently wider than the temperature interval of martensite transformation. At the end of relaxation, the repeated increase of temporary stresses occurred, but in 4 h, the residual stresses reached only 117 MPa. As subsequent investigations showed, these low levels of residual stresses are associated with the formation of a crack network in the work portion of the specimen.

Metallographic examination showed, that, as a result of thermostrain process, the relief was formed at the polished surface of the specimen, characterizing the microplastic strain. More intensive plastic strain is observed in the area near the notch. Hence, two types of the relief are formed, as shown in Fig. 10A: Black contour bands (1) with traces of grain boundary slipping and light, thin bands with traces of intergranular strain. Parallel light, needle-shaped thin bands, forming pockets (2) with typical zigzags (3), represent the traces of shears, which occurred in the process of martensite transformation, and thin, wavy lines (4) represent the traces of slip. In grain boundary slipping at grain meeting points the strain centers (5) are formed, the result of microstress concentration and, correspondingly, local plastic strain. Increase in plastic strain near the nonmetallic inclusion (6) is observed. It is also observed that the short bands of intensive strain pass from the boundary into the grain (7). Migration displacements (8) are also noted.

At some distance from the notch, the intensity of microplastic strain traces decreases, and the bands of grain boundary slipping become thinner. However, in some areas near the three grain meeting point, grain boundary slipping is sufficiently developed (Fig. 10B, 1 and 2). The turning of these bands into grain (3) takes place, associated with the presence of obstacles at the boundaries. Inside the grains, two types of already described needle-shaped bands, which are the traces of shears in martensite transformation, are clearly observed. The traces of sufficient local shears are seen in the pockets (4) of the needle-shaped bands near the three grains meet point and grain boundary band of slipping.

Branching of bands, which are the traces of shear processes, and their moving from the supposed boundaries into the grain body (Fig. 10C, 1 and 2), result in uneven microplastic strain both in boundary areas and inside the grains — Fig. 10C, area 3. Microplastic strain is located near the nonmetallic inclusions (Fig. 10D, areas 1 and 2), placed on the bands of grain boundary slipping.

Nonmetallic inclusions with sufficiently high concentration of stresses are the centers of the development of grain boundary slipping — Fig. 10E, area 1. Note in Fig. 10E, area 2, the local shearing processes are developed because of nonmetallic inclusion.

Figure 10F also shows the variety of plastic strain under the heating-cooling conditions. Here, very wide-contour bands of the slipping are absent; however, traces of several bands are sufficiently clear, observed in area 1, the location of which approximates the boundary migration. They are probably relief bands, traces of shearing processes that occurred in different stages of WTSC, but more contrast band (black contour) appeared in these under the conditions of temporary stress relaxation at temperatures close to T_{rb}. Nonmetallic inclusions, as was already indicated, cause the increase of shearing processes (Fig. 10F, areas 2 and 3), and grain boundary slipping causes the formation of clusters of acicular traces of shears (4). Sufficient unevenness of plastic strain in separate microvolumes is observed (5).

Comparison between the diagram of the change of AE pulses in WTSC of temporary stresses and the picture of microrelief at the surface of the specimen shows that the intensive relaxation of stresses is associated with more drastic activation of microplastic strain by intergranular slipping and intragranular shear

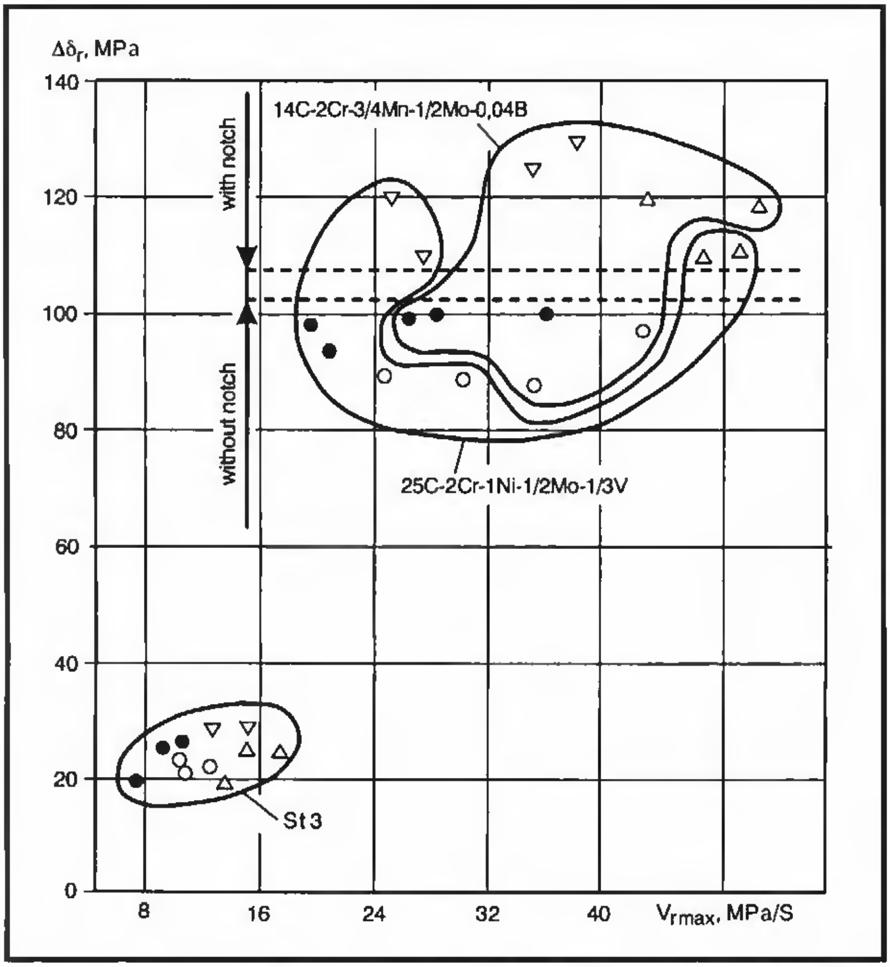

Fig. 7 — Effect of steel alloying system on the dependence of $\Delta\sigma_r$ relaxation characteristic on the rate of relaxation $V_{r\,max}$. (Designations, see Fig. 5.)

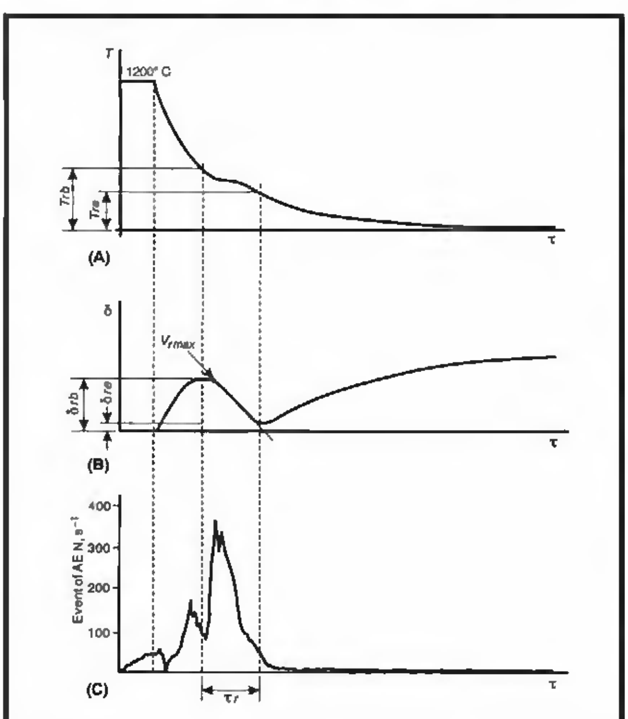

Fig. 8 — Acoustogram (C) for steel 25C-2Cr-1Ni-1/2Mo-1/3V before and during the development of intensive relaxation of stresses (A, B).

formation. Hence, when the relaxation-rate is increased, the rate of microplastic strain increases.

After the end of the first stage of examination, the working surface of the specimen was repeatedly ground and polished until the total removal of strain relief, and then was etched in a 4% alcohol solution of nitric acid to reveal the microstructure.

In the area near the notch, where intensive grain boundary slipping is observed (Fig. 10A), the boundaries of grains are the relatively wide, light lines — Fig. 11. Their etching sensitivity is determined by the level of structural imperfection and contaminaton associated with segregation of carbon and impurity elements (phosphorus, sulphur) at these boundaries. It is characteristic of the coarse grains located in the HAZ of welded joints near the weld interface.

The intergranular structure is martensite and ferrite and the oriented secondary phase location of these structural components coincides with the relief of microplastic strain at the polished surface.

The intergranular submicro- and microcracks (Fig. 11) form along the light boundaries that coincide with the most intensive grain houndary slipping lines.

The weak boundaries of the coarse grains (near the weld interface of the welded joint) form during the entire cycle of heating-cooling the HAZ metal (Ref. 5). The degree of weakening is determined by cycle peculiarities and the steel composition. Over a wide temperature range, the complex processes of intra- and intergranular plastic strain develop, which cause high mobility of the crystalline structure defects, the acceleration of diffusion and the restructuring.

Due to the continuous process of intra- and intergranular strain, the high density of movable dislocations and the free energy stored in strain persist by the moment of the beginning of austenite decomposition. Martensitic transformation with the intensive grain boundary slipping and the impact effect of the martensite needles on the grain boundaries accompanied by the formation of serrations, microcavities and pores causes the extra weakening of the interatomic bonds and formation of microstresses at the grain boundaries.

Therefore, initiation of cold crack nuclei under the conditions of a welding thermal strain cycle requires the combination of the two main factors. The first is formation of the coarse austenite grain boundaries under the conditions of the intensive intragranular and grain-boundary plastic strains, as well as segregation of impurities along the grain boundaries and the resulting considerable weakening of the interatomic bond. The second is the drastic intensification of the temporary stress relaxation process as a result of the shear processes of local overstress formation in the areas of the defected structure, these overstresses being the sources of fracture process development.

From the data obtained, it is possible to estimate the effect of hydrogen on cold-crack formation. In cooling, its distribution in the austenite grains becomes more nonuniform and its concentration increases at the grain boundaries within the zone of the most significant structural distortions, at the location of the segre-

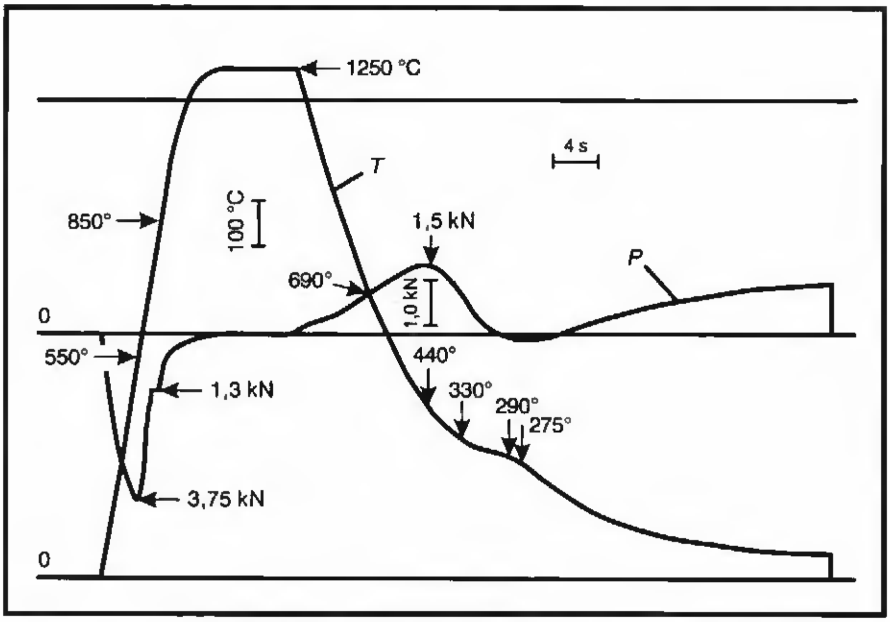

Fig. 9 — Temporary dependence of temperature T and force P in the specimen, subjected to the effect of WTSC in restrained condition.

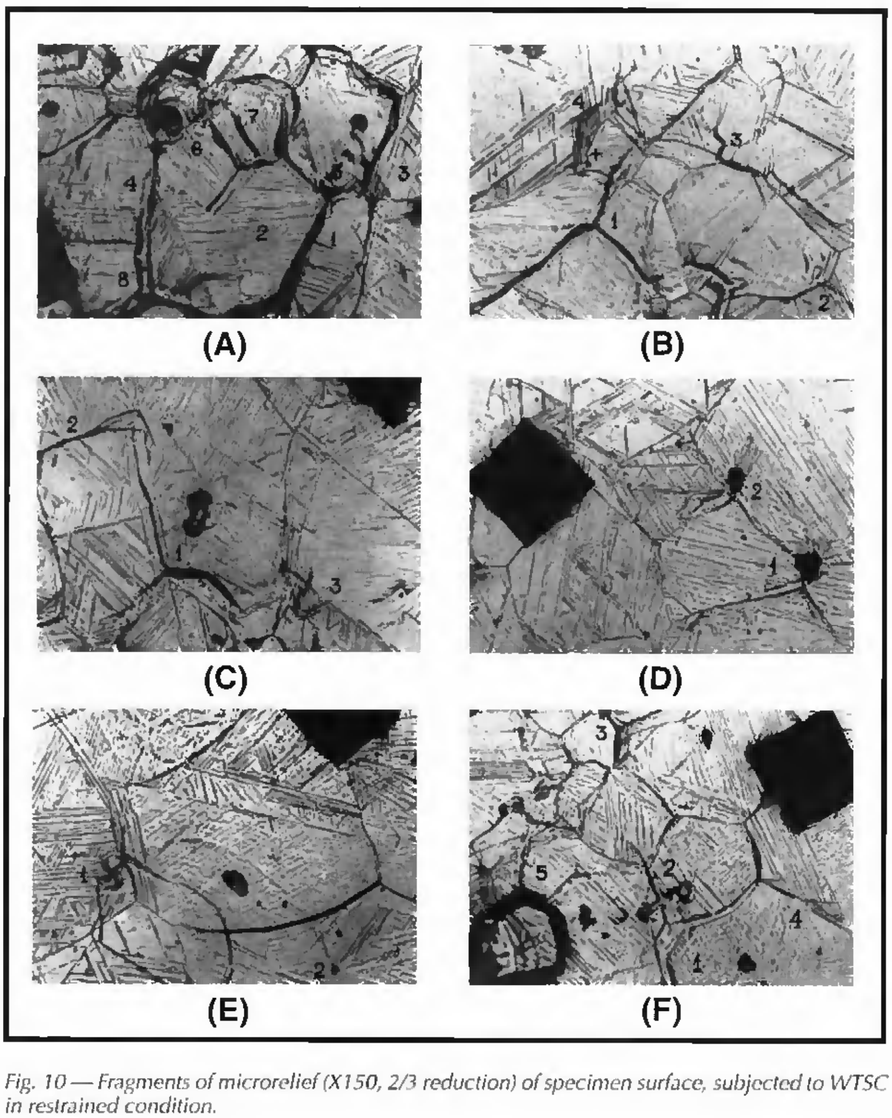

Fig. 10 — Fragments of microrelief (X150, 2/3 reduction) of specimen surface, subjected to WTSC in restrained condition.

gating impurities and the nonmetallic inclusions (Refs. 5–7). Concentration of hydrogen in the grain boundary zone causes the additional decrease in the interatomic bonds. In $\gamma \rightarrow \alpha$ transformation a part of hydrogen is precipitated from solid solution. The rate of its redistribution under the WTSC conditions will be determined by drift diffusion related to the rate of the shear processes taking place in martensitic transformation and subsequent cooling. The drift diffusion of hydrogen is known to occur at a high rate and to promote the considerable nonuniformity of its distribution in metal with maximum concentration at the grain boundaries (Refs. 5–7).

When microtears form at the grain boundaries, hydrogen is adsorbed at the newly formed surface and reduces the effective surface energy near the tear apex, thus favoring the crack propagation.

The active effect of hydrogen on the process of cold-crack formation is observed in welding of low- and medium-alloyed steels with different carbon content. However, its effect is different. The grain boundary microstructural heterogeneity of the HAZ austenite grain increases with the growth of carbon content of steel from 0.20 to 0.40% (by the beginning of $\gamma \rightarrow \alpha$ transformation). Here, one sees an increase in the total embrittlement effect associated with the grain boundary impurity segregation and hydrogen whose concentration in the boundary region of the coarse austenite grain can be high enough even at its comparatively low total content. The joint embrittlement effect of said factors, combined with intensive process of microplastic strain in martensitic transformation, determines the probability of cold cracking.

The grain boundary microstructural heterogeneity of HAZ austenite grains and the intensity of microplastic strain in the process of $\gamma \rightarrow \alpha$ transformations decrease with the decrease of the carbon content (less than 0.20% carbon). Here, the role of the diffusible hydrogen (its content and diffusion rate) in the cold-crack formation becomes decisive. The formation of the nucleus microcracks requires — due to diffusion and other transport mechanisms (Refs. 5–7) — the creation of the sufficiently high concentration of the atomic hydrogen in some microvolumes of the HAZ. Since its absorption at the newly formed crack tip requires some time, the crack propagation has the pulse (sudden) character. Here, metal gradually fails at stresses that are considerably lower than in the absence of hydrogen.

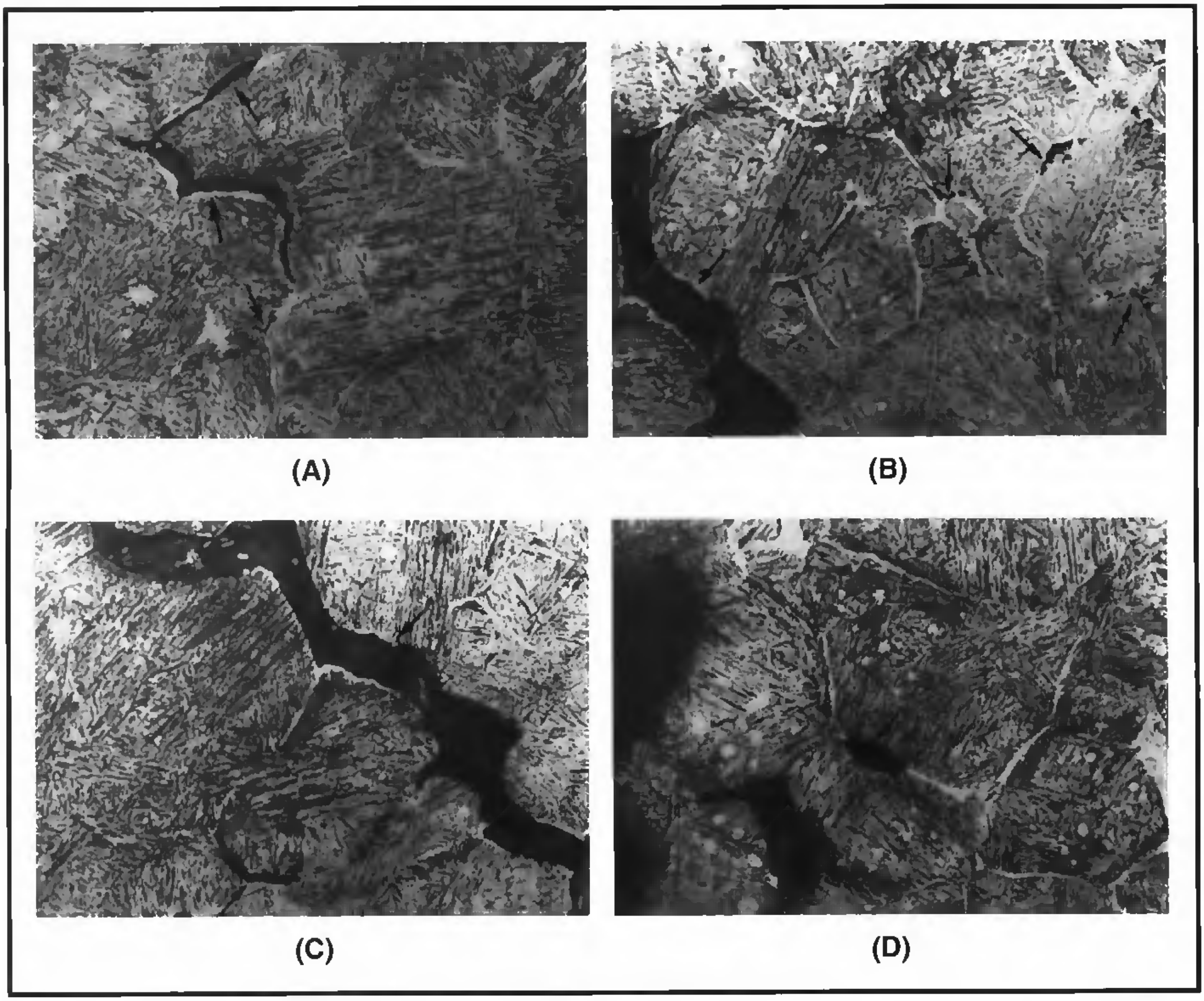

Fig. 11 — Microstructure (X150, 2/3 reduction) of specimen, subjected to WTSC in restrained condition.

Conclusions

1) The procedure suggested allows study of the main thermal strain indices that determine probability of cold cracking in welding of low- and medium-alloyed steels.

2) Chemical composition of steels and peculiarity of inter- and intragranular plastic strain of the restrained specimens under WTSC conditions determine the structural imperfection of the coarse austenite grain boundaries (HAZ) which, combined with the intensive relaxation of temporary stresses in the process of structural transformations, condition the probability of cold-crack initiation and propagation.

3) Suggested is the parameter M_r of the intensive stress relaxation during structural transformations to estimate susceptibility of steels to cold cracking.

4) Hydrogen plays the active role in cold cracking of the HAZ.

References

1. Compendium of weld metal microstructures and properties: submerged-arc welds in ferritic steel. 1985. Prepared for Com. IX of the Intern. Inst. of Welding by Sub-Comm. IXJ. Abington Hall a.o., IIW, XVI, p. 111.

2. Inagaki, M., Nishikawa, J., Minematsu, H., Kosuge, S., and Nakamura, H. 1973. Development and its application of weld thermal restraint stress and strain-cycles simulator. *Trans. Japan Welding Society*, 4(1): 3–18.

3. Nemec, J. 1963. Rigidity of strength of steel parts. Praha, Publishing House of Czechoslovak Academy of Sciences, p. 771.

4. *Acoustic emission and its application for the non-destructive testing in nuclear power engineering*. 1980. Ed. by K. B. Vakar-M, Atomizdat, p. 216.

5. Savage, W. F., Nippes, E. F., and Sawhill, I. M. 1976. Hydrogen-induced cracking during implant testing of alloy steels. *Welding Journal* 55 (12): 400-s to 407-s.

6. Savage, W. F., Nippes, E. F., and Szekeres, E. S. 1976. A study of weld interface phenomena in a low-alloy steel. *Welding Journal* 55 (9): 276-s to 283-s.

7. Watkinson, F. 1969. Hydrogen cracking in high-strength weld metals. *Welding Journal* 48: 417-s to 424-s.